arXiv:1402.4021v3 [cond-mat.soft] 11 Aug 2014

Inherent variability in the kinetics of autocatalytic protein self-assembly

Juraj Szavits-Nossan,* Kym Eden,† Ryan J. Morris, Cait E. MacPhee, Martin R. Evans, and Rosalind J. Allen‡
SUPA, School of Physics and Astronomy, University of Edinburgh, Mayfield Road, Edinburgh EH9 3JZ, United Kingdom

In small volumes, the kinetics of filamentous protein self-assembly is expected to show significant variability, arising from intrinsic molecular noise. This is not accounted for in existing deterministic models. We introduce a simple stochastic model including nucleation and autocatalytic growth via elongation and fragmentation, which allows us to predict the effects of molecular noise on the kinetics of autocatalytic self-assembly. We derive an analytic expression for the lag-time distribution, which agrees well with experimental results for the fibrillation of bovine insulin. Our expression decomposes the lag time variability into contributions from primary nucleation and autocatalytic growth and reveals how each of these scales with the key kinetic parameters. Our analysis shows that significant lag-time variability can arise from both primary nucleation and from autocatalytic growth, and should provide a way to extract mechanistic information on early-stage aggregation from small-volume experiments.

PACS numbers: 87.14.em, 87.15.nr, 87.18.Tt, 05.10.Gg

The self-assembly of protein molecules into amyloid fibrils is associated with many degenerative diseases [1], but also presents potential opportunities for the development of new materials [2]. In both cases it is of outstanding importance to identify the specific microscopic steps responsible for amyloid aggregation, especially in its early stages. An important success of recent biophysical work has been to show that *in vitro* kinetic data for amyloid fibril self-assembly can often be described by deterministic mechanistic models [3–11]. However, it is unclear how far the results of these large-volume experiments can be translated to clinically relevant intracellular aggregation phenomena, which occur in far smaller volumes.

In large-volume *in vitro* experiments (typically 100-1000 μl), measurements of the total mass of aggregated (fibrillar) protein as a function of time typically produce sigmoidal curves, as in figure 1(a) [2]. These data show an initial lag phase in which no aggregated protein is detectable, followed by a rapid growth phase, terminating in a plateau once all the protein is in the aggregated form. In large volumes, these characteristic sigmoidal growth curves can often be well fitted by deterministic kinetic models involving homogeneous primary nucleation (Fig. 1(c), I), filament elongation by monomer addition (Fig. 1(c), II) and autocatalysis via filament fragmentation (Fig. 1(c), III) [2, 7, 12–14] – although the contributions of primary nucleation and autocatalytic growth in the early stages of aggregation are often poorly distinguished [15]. Importantly, these models lead to analytical predictions for scaling behavior; for example, if autocatalysis is dominant, the mean lag time scales as the inverse square root of the product of the protein concentration, elongation and fragmentation rates [7].

In a clinical context, however, fibril formation happens in much smaller volumes, on the scale of a human cell (typically $500 - 3000$ fl). In small volumes, the stochastic nature of the underlying chemical reactions ("intrinsic molecular noise") is expected to become important, leading to inherent variability in the aggregation kinetics. Fig. 1(b) shows the results of replicate kinetic Monte Carlo simulations of a stochastic version of the autocatalytic growth model [17] in a volume of 830 fl. These simulations predict significant variability in the lag time. Lag-time variability has also been observed in recent pioneering experiments on bovine insulin fibril formation in micro-droplets [18], as well as in classic small-volume ex-

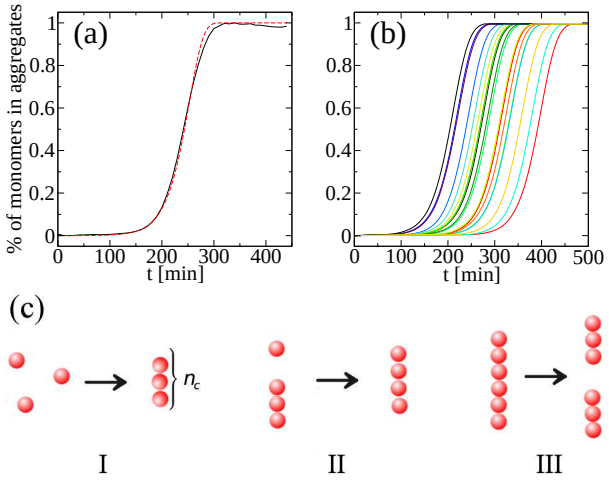

FIG. 1: (a) Experimental kinetic curve (black line) for the aggregation of bovine insulin in a volume of 100 μl from our own experiment, fitted to the theoretical prediction of a model [7] involving primary nucleation, elongation and fragmentation (dashed red line); for full experimental details, see the Supplemental Material. (b) Kinetic curves obtained from kinetic Monte Carlo simulations of a stochastic version of the same model [7, 17] and the fit parameters extracted from (a), but for a much smaller volume of 830 fl. (c) Schematic illustration of: (I) primary nucleation, (II) elongation via polymerization and (III) fragmentation. The critical nucleus size for primary nucleation is denoted by n_c.

periments on the polymerization of sickle cell hemoglobin [19–21]. Theoretical models which explain such data should provide a powerful tool for probing the mechanisms involved in early-stage aggregation. In particular, an important question concerns the relative roles of primary nucleation (Fig. 1(c), I) and autocatalytic growth (Fig. 1(c), II and III) in determining the lag-time distribution for amyloid fibril formation. So far, however, analytic predictions for lag-time distributions have been achieved only for models that do not fully take into account autocatalytic growth [22, 23].

In this paper, we present an analytic prediction for the lag-time distribution, for a stochastic model of filamentous protein self-assembly that includes primary nucleation, irreversible filament elongation and autocatalysis via fragmentation. We show that our prediction is in agreement with recent data for bovine insulin fibril formation in micro-droplets [18]. This analytical solution allows a decomposition of the lag time variability into contributions from primary nucleation and autocatalytic growth, and reveals how each of these scales with the key kinetic parameters.

A Coarse-Grained Model for Autocatalytic Protein Self-Assembly. Deterministic kinetic models for amyloid fibril self-assembly usually consist of dynamical equations for the mean number of fibrils $\langle n_i \rangle$ of a given length $i \geq n_c$, where n_c is the size of the smallest growth-competent fibril (the "nucleus") [2, 7, 12–14] [24]. For a model including homogeneous nucleation, irreversible elongation and fibril fragmentation (Fig. 1(c), I-III), these equations are non-linear, but various approximations have been successfully employed to obtain their full time-dependent solution [7, 12–14]. The stochastic version of this model, where the number of each species n_i is allowed to fluctuate is, however, analytically intractable, although it can be simulated numerically as we have done in Fig. 1(b).

To obtain an analytic prediction for the lag-time distribution, we coarse-grain the model, while retaining the key processes of nucleation, elongation and fragmentation. Rather than tracking the full distribution of fibril lengths, we track only the total number of fibrils $n = \sum_i n_i$ and the number of monomers in aggregates $m = \sum_i i n_i$, but treat them as discrete random variables, which can fluctuate due to intrinsic noise. This coarse-graining, which amounts essentially to summing over fibril lengths in the full model [25], results in the following set of possible transitions between states n, m of the system:

$$n, m \to \begin{cases} n+1, m+n_c & \text{at rate } \alpha[c(t)]/\epsilon \quad (1a) \\ n, m+1 & \text{at rate } 2k_+ c(t) n \quad (1b) \\ n+1, m & \text{at rate } k_f m \quad (1c) \end{cases}$$

Primary nucleation is modeled by (1a) as an one-step process in which a new filament (called a "nucleus") is created instantaneously from n_c free monomers at rate $\alpha[c(t)]\epsilon$. The rate α is assumed to depend on the molar concentration of free monomers $c(t)$ and $\epsilon = 1/(VN_A)$, where V is the volume and N_A is Avogadro's constant. Transition (1b) represents filament growth by monomer addition at rate $2k_+c(t)$; the factor of 2 accounts for the fact that filaments can grow at both ends. Transition (1c) represents fragmentation; this amounts to an autocatalytic creation of new fibrils from existing ones at rate k_f; the probability that any given fibril breaks is assumed to be proportional to its length. Although this assumption is somewhat simplistic [26], we have also studied a model where fibrils break more frequently at their ends [27]. This latter model, which is presented in the Supplemental Material, also obeys detailed balance by including backward reactions such as re-joining of fragmented fibrils and loss of monomers at fibril ends; however, none of these changes were found to affect the early-stage aggregation phenomena studied here [16, 28]. In the rest of the paper we will further simplify the model by neglecting monomer depletion, which amounts to approximating the free monomer concentration $c(t)$ by c_{tot}; this has little effect on the lag phase.

The probability distribution $P_{n,m}(t)$ for a given n and m obeys the following master equation

$$\begin{aligned} \frac{d}{dt}P_{n,m} = (\alpha/\epsilon)P_{n-1,m-n_c} + \mu n P_{n,m-1} \\ + \lambda m P_{n-1,m} - (\alpha/\epsilon + \mu n + \lambda m)P_{n,m}, \end{aligned} \quad (2)$$

where $\alpha \equiv \alpha(c_{tot})$, $\mu \equiv 2k_+c_{tot}$ and $\lambda \equiv k_f$. Starting with an initial condition $P_{n,m}(0) = \delta_{n,n_0}\delta_{m,m_0}$, we aim to solve for $P_{n,m}(t)$, and then to find the probability distribution for the lag time, i.e. for the time needed for the number of aggregated monomers m to reach some predefined threshold m_T, which we define as 10% of the total number of monomers (which is given by c_{tot}/ϵ, assuming that c_{tot} is measured in moles per unit volume).

Analytic Solution for the Probability Distribution $P_{n,m}$. In order to obtain an analytic solution, we replace the master equation (2) with a corresponding Fokker-Planck equation via the linear noise approximation (LNA), also known as Van Kampen's system size expansion [29, 30]. The LNA assumes that n and m can be decomposed into deterministic and fluctuating parts,

$$n = N_A V \phi(t) + \sqrt{N_A V} x_1 \quad (3a)$$

$$m = N_A V \psi(t) + \sqrt{N_A V} x_2, \quad (3b)$$

where the fluctuating parts x_1 and x_2 are scaled by $\sqrt{N_A V}$, and are assumed to be small compared to the deterministic terms. The deterministic parts $\phi(t)$ and $\psi(t)$, expressed in units of concentration (here moles per

unit volume), solve the following differential equations:

$$\frac{d\phi}{dt} = \lambda\psi + \alpha, \quad \phi(0) = \epsilon n_0 \equiv \phi_0 \tag{4a}$$

$$\frac{d\psi}{dt} = \mu\phi + \alpha n_c, \quad \psi(0) = \epsilon m_0 \equiv \psi_0. \tag{4b}$$

Equations (4a) and (4b) may be solved to yield

$$\phi(t) = \sqrt{\frac{\lambda}{\mu}}\Psi_0 \sinh(\tau) + \Phi_0 \cosh(\tau) - \frac{\alpha n_c}{\mu} \tag{5a}$$

$$\psi(t) = \sqrt{\frac{\mu}{\lambda}}\Phi_0 \sinh(\tau) + \Psi_0 \cosh(\tau) - \frac{\alpha}{\lambda}. \tag{5b}$$

where we have adopted the following notation: $\tau = \sqrt{\mu\lambda}t$, $\Phi_0 = \phi_0 + \alpha n_c/\mu$ and $\Psi_0 = \psi_0 + \alpha/\lambda$. Equations (5a) and (5b) describe the time evolution of the mean concentrations of fibrils and aggregated protein, respectively, at early times. Solving $\psi(T) = m_T\epsilon$, where m_T is the threshold concentration, yields the mean lag time T

$$T = \frac{1}{\sqrt{\mu\lambda}} \ln \frac{D + \sqrt{D^2 - \Psi_0^2 + (\mu/\lambda)\Phi_0^2}}{\Psi_0 + \sqrt{\mu/\lambda}\Phi_0}, \tag{6}$$

where $D = \alpha/\lambda + m_T\epsilon$. Eq. (6) is a good approximation to the lag time reported in [7] and predicts the same $T \propto (k_+ c_{tot} k_f)^{-1/2}$ scaling.

To determine the effects of intrinsic noise, we now turn to the fluctuating parts x_1 and x_2, which are governed by the following Fokker-Planck equation for the probability density $P(x_1, x_2, t)$,

$$\frac{\partial P}{\partial t} = -\sum_i \frac{\partial}{\partial x_i}(A_i P) + \frac{1}{2}\sum_{i,j}\frac{\partial^2}{\partial x_i x_j}(B_{ij}P) \tag{7}$$

where we assumed that $P(x_1, x_2, 0) = \delta(x_1)\delta(x_2)$. The drift vector $\vec{A}$ and the diffusion matrix B are given by

$$\vec{A} = \begin{pmatrix} \lambda x_2 \\ \mu x_1 \end{pmatrix}, \quad B = \begin{pmatrix} \lambda\psi + \alpha & \alpha n_c \\ \alpha n_c & \mu\phi + \alpha n_c^2 \end{pmatrix}. \tag{8}$$

Equation (7) describes a two-variable (time-dependent) Ornstein-Uhlenbeck process which can be solved by standard techniques [30] and yields a bivariate Gaussian distribution with zero mean and time-dependent covariance matrix $\Sigma_{ij} = \langle x_i x_j \rangle$. To calculate the lag time distribution we only need to know $\Sigma_{22} = \langle x_2(t)^2 \rangle$; the time-dependence of the other matrix elements can be found in the Supplemental Material.

Lag Time Distribution. Building on these results, we now obtain an analytic expression for the lag time distribution $L(t)$. This is essentially a first-passage time problem; to calculate $L(t)$, we look for all events such that m has *just* exceeded m_T at a time t, given that it will exceed m_T eventually,

$$L(t) = \frac{\frac{d}{dt}\text{Prob}[m > m_T, t]}{\text{Prob}[m > m_T, t \to \infty]}. \tag{9}$$

The probability $\text{Prob}[m > m_T, t]$ can easily be calculated by integrating $P(x_1, x_2, t)$ and reads

$$\text{Prob}[m > m_T, t] = \frac{1}{2}\text{erfc}\left(\frac{m_T\epsilon - \psi(t)}{\sqrt{2\epsilon\langle x_2(t)^2\rangle}}\right), \tag{10}$$

A lengthy but straightforward calculation for $\langle x_2(t)^2 \rangle$ gives

$$\begin{aligned}\langle x_2(t)^2\rangle &= \cosh(2\tau)\left[\frac{1}{6}\left(\Phi_0\frac{\mu}{\lambda} + \Psi_0\right) + \frac{\alpha n_c}{2\lambda}\right] \\ &+ \sinh(2\tau)\sqrt{\frac{\mu}{\lambda}}\left[\frac{\Phi_0 + \Psi_0}{3} + \frac{\alpha n_c(n_c - 1)}{4\mu}\right] \\ &+ \frac{\cosh\tau}{3\lambda}(\lambda\Psi_0 - 2\mu\Phi_0) + \frac{\sinh\tau}{3}\sqrt{\frac{\mu}{\lambda}}(\Phi_0 - 2\Psi_0) \\ &- \frac{\alpha n_c(n_c - 1)t}{2} + \frac{1}{2}\left(\Phi_0\sqrt{\frac{\mu}{\lambda}} - \Psi_0 - \frac{\alpha n_c}{\lambda}\right).\end{aligned} \tag{11}$$

It now proves useful to introduce a new variable $r(t)$,

$$r(t) = \frac{\psi(t) - m_T\epsilon}{\sqrt{\epsilon\langle x_2(t)^2\rangle}} \tag{12}$$

which measures the deviation of the mean fibril concentration ($\psi(t)$) from the threshold ($m_T\epsilon$), scaled by the root mean square of $m\epsilon - \psi(t)$. Using this variable, we combine expressions (9), (10) and (11) to give our central result: an analytical expression for the lag time distribution in the linear noise approximation of the master equation (2), which takes the form of a Gaussian in r in the range $-\infty < r < r(\infty)$ [25],

$$L(t)dt = \frac{dr/dt}{\sqrt{2\pi}Z}e^{-\frac{r(t)^2}{2}}dt = \frac{1}{\sqrt{2\pi}Z}e^{-\frac{r^2}{2}}dr, \tag{13}$$

where $Z = \text{erfc}(-r(\infty)/2)$. Importantly, Eq. (13) allows us to easily calculate moments of the lag time distribution. For example, to calculate the mean lag time $\langle t \rangle$ and its standard deviation σ, we express t and t^2 as functions of r and perform a Taylor expansion around $r = 0$ (see the Supplemental Material for details). This gives

$$\langle t \rangle \approx T \quad \text{and} \quad \sigma \approx \frac{\sqrt{\epsilon\langle x_2^2(T)\rangle}}{\mu\phi(T) + \alpha n_c}. \tag{14}$$

For most proteins, the fragmentation rate $\lambda \equiv k_f$ is much smaller than the net fibril elongation rate $\mu \equiv 2k_+ c_{tot}$; i.e. $\lambda \ll \mu$. If we also assume that no fibrils are present at time $t = 0$ ($\phi_0 = \psi_0 = 0$), we can write a simpler expression for the standard deviation of the lag time,

$$\sigma = \frac{(2/3)^{1/2}}{(\mu\lambda)^{1/4}(\alpha N_A V)^{1/2}}. \tag{15}$$

Remarkably, Eq. (15) implies that the lag time variance scales in a simple way with the model parameters. Like the mean lag time, the variance is predicted to scale as

$\sqrt{\mu\lambda} \sim \sqrt{k_f k_+}$. Interestingly, however, the mean and variance of the lag time may show different dependencies on the protein concentration c_{tot}; while the mean scales as $c_{tot}^{-1/2}$, in expression (15) for the variance this factor (which arises from μ) is multiplied by an additional factor due to the c_{tot}-dependent nucleation rate α; the scaling of this factor depends on the nucleus size n_c.

It is important to note that results (13)-(15) only hold in the regime dominated by growth, where fluctuations in n and m are much smaller than their averages, *for all times*. In contrast, for slow nucleation rates, a significant portion of the lag time is spent waiting for the first nucleus to be spontaneously created, which is a fluctuation-driven process. We take this into account by convolving $L(t-t')$ with the waiting time distribution $(\alpha/\epsilon)\exp(-\alpha t'/\epsilon)$ for the primary nucleation event, to give

$$L_1(t) = (\alpha/\epsilon)\int_0^t dt' e^{-(\alpha/\epsilon)t'} L(t-t'), \qquad (16)$$

where in the expression for $L(t-t')$ we set $\phi(t') = \epsilon$ and $\psi(t') = n_c\epsilon$ (i.e. assume one fibril of size n_c at time t'). Figure 2 shows that the lag-time distributions predicted by Eqs. (13) and (16) are in good agreement with the results of stochastic simulations of the full model (which takes into account fibril lengths), for several values of the primary nucleation rate α. For relatively fast nucleation rates, our "bare" LNA prediction $L(t)$ (Eq. 13) is sufficient (main plots in Figure 2); for slower nucleation rates (inset in Fig. 2)), (16) should be used instead (inset to Fig. 2).

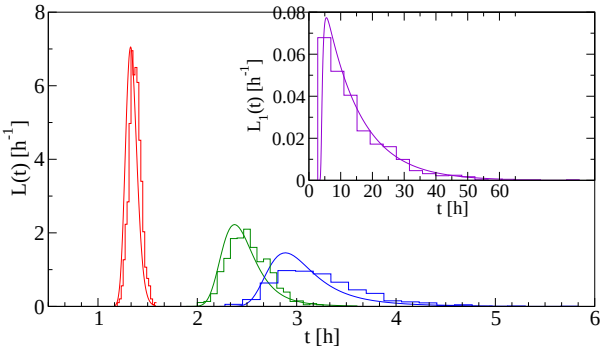

FIG. 2: The lag-time distribution $L(t)$ for several values of α, compared to that obtained by running 1000 independent kinetic Monte Carlo simulations of the full stochastic model (in which individual fibril lengths are resolved) [17]. From left to right: $\alpha = 50$ (full line), 5 (dashed line), 1.5 (dot-dashed line), all in units of 10^{-15} mol/(ls). Inset: $L_1(t)$ (dashed line) compared to simulations for $\alpha = 5\cdot 10^{-17}$ mol/(ls). The other parameters are: $V = 830$ fl, $M_T = 10\%$ of c_{tot}, $c_{tot} = 100$ μmol/l, $n_c = 2$, $k_+ = 5\cdot 10^4$ l/(mol s) and $k_f = 3\cdot 10^{-8}$ s^{-1}.

For slow nucleation rates, we can separate the contributions of primary nucleation and autocatalytic growth to the lag time variance in a simple way. Assuming $L(t)$ can be replaced by a Gaussian in t, we can use (14) to compute the integral in (16) in a closed form which reveals that $L_1(t)$ has mean T_1 and standard deviation σ_1 given by

$$T_1 = \frac{\epsilon}{\alpha} + T, \quad \sigma_1 = \sqrt{\left(\frac{\epsilon}{\alpha}\right)^2 + \sigma^2}. \qquad (17)$$

Thus the lag-time variance is given by a simple sum of the variance of the exponential waiting time distribution for the primary nucleation event, and the contribution from autocatalytic growth, given by Eq. (15).

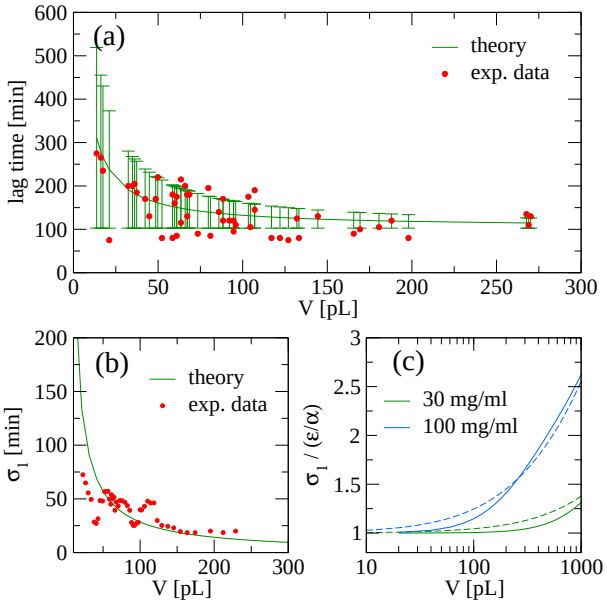

FIG. 3: (a) Volume dependence of the lag time for the aggregation of bovine insulin in microdroplets of varying volume (red dots) [18], compared to the mean (solid line) and the standard deviation (error bars) from Eq. 17, using the following values, which were obtained from Ref. [18]: $T = 104$ min, $\alpha = 1/(1.7\cdot 10^{-7} N_A)$ mol/(l s), $k_+ = 8.9\cdot 10^4$ l/(mol s), $k_f = 2\cdot 10^{-8}$ s^{-1} and assuming $n_c = 2$. (b) Corresponding volume dependence of the standard deviation; the red dots are 6-point moving standard deviation from the experimental data, and the solid green line is from (17). (c) Theoretical predictions for the standard deviation σ_1 as a function of volume, relative to ϵ/α. The green (lower) lines correspond to the protein concentration 30 mg/ml used in Ref. [18], while the blue (upper) lines are for a higher protein concentration, 100 mg/ml, assuming that $\alpha(c_{tot}) \propto {c_{tot}}^{n_c}$ [7]. In both cases, the dashed lines correspond to (17) while the solid lines are calculated numerically from (16).

Comparison with Experimental Results for Bovine Insulin. So far, the only available experimental data on amyloid fibril nucleation in small volumes is that of Knowles *et al.*, who tracked the fibrillation of bovine insulin in 52 micro-droplets of volumes in the range $10-300$ pl, using ThT fluorescence [18]. Fig. 3(a) shows the resulting lag times (red dots) as a function of droplet vol-

ume, compared to our theoretical prediction; the green line shows the mean lag time T_1, and the error bars show the standard deviation σ_1, from Eq. (17). No fitting parameters were used in this plot; rather the parameters k_+, k_f and α were taken directly from the measurements of Ref. [18] [32]. While there are not enough experimental data points to plot a lag-time distribution for any given volume, Fig. 3(a) shows that the variability observed in the experiments is consistent with our theory. This is further evidenced in Fig. 3(b), where we plot directly the volume-dependence of the standard deviation.

We can also use our result, Eq. (17), to explore the relative contributions of primary nucleation and autocatalytic growth to the lag-time variability. Fig. 3(c) shows our theoretical prediction for the standard deviation σ_1, relative to that for primary nucleation only, ϵ/α. The relative contribution of autocatalytic growth increases strongly as the volume increases (although the total variability decreases with V). For the protein concentration of 30 mg/ml used in Ref. [18], primary nucleation is the main contributor. However, for higher protein concentrations, we predict that autocatalytic variability becomes significant even at smaller volumes, on the scale of a human cell.

Conclusion. We have presented an analytic expression for the lag time distribution, for a stochastic model of autocatalytic protein self-assembly which includes nucleation, elongation and fragmentation. Our solution provides simple scaling relations for the contributions to lag-time variability due to primary nucleation and autocatalysis, both of which can be significant under realistic conditions. The implications of molecular noise for variability in clinical outcomes between individuals, as well as the possible connection to variability between replicates in large volume experiments [33] present interesting and important directions for future work.

We thank Tuomas Knowles for kindly providing the data from Ref. [18] which we have used in Fig. 3 and Line Jourdain for discussions in the early stages of this work. KE and JSN contributed equally to this work. This research was supported by EPSRC under grant number EP/J007404/1. KE was supported by an EPSRC DTA studentship and RJA was supported by a Royal Society University Research Fellowship.

* Electronic address: jszavits@staffmail.ed.ac.uk
† Electronic address: k.eden@ed.ac.uk
‡ Electronic address: rallen2@staffmail.ed.ac.uk

[1] F. Chiti and C. M. Dobson, *Annu. Rev. Biochem.* **75**, 333-66 (2006)
[2] J. E. Gillam and C. E. MacPhee, *J. Phys.: Condens. Matter* **25** 373101 (2013)
[3] A. Wegner, *Nature* **296**, 266-267 (1982)
[4] A. Wegner and P. Savko, *Biochemistry* **21**, 1909-1913 (1982)
[5] F. Ferrone, Meth. Enzymol. **309**, 256-274 (1999)
[6] M. Tanaka, S. R. Collins, B. H. Toyama and J. S. Weissman, *Nature* **442**, 585 (2006)
[7] T. P. J. Knowles et al., *Science* **326** 1533-7 (2009)
[8] F.A. Ferrone, J. Hofrichter, H.R. Sunshine, W.A. Eaton, *Biophy. J.* **32**(1), 361380 (1980)
[9] M. F. Bishop and F. A. Ferrone, *Biophys. J.* **46**, 631-44 (1984)
[10] A. M. Ruschak and A. D. Miranker, *Proc. Natl Acad. Sci. USA* **104**, 12341-6 (2007)
[11] L. Jean, C. F. Lee, C. Lee, M. Shaw and D. J. Vaux, *FASEB J.* **24**, 309-17 (2010)
[12] S. I. A. Cohen, M. Vendruscolo, M. E. Welland, C. M. Dobson, E. M. Terentjev and T. P. J. Knowles, *J. Chem. Phys.* **135**, 065105 (2011)
[13] S. I. A. Cohen, M. Vendruscolo, C. M. Dobson, and T. P. J. Knowles, *J. Chem. Phys.* **135**, 065106 (2011)
[14] S. I. A. Cohen, M. Vendruscolo, C. M. Dobson, and T. P. J. Knowles, *J. Chem. Phys.* **135** 065107 (2011)
[15] J.P. Bernacki and R.M. Murphy, *Biophy. J.* **96** 2871-87 (2009)
[16] L. Hong and W.-A. Yong, *Biophys. J.* **104**, 533-540 (2013)
[17] R. J. Morris, K. Eden, R. Yarwood, L. Jourdain, R. J. Allen and C. E. MacPhee, *Nat. Commun.* **4**, 1891 (2013)
[18] T. P. J Knowles et al., *Proc. Natl Acad. Sci. USA* **108**(36), 1474614751 (2011)
[19] F. A. Ferrone, J. Hofrichter, W. A. Eaton, *J. Mol. Bio.* **183**(4), 591-610 (1985)
[20] F. A. Ferrone, J. Hofrichter, W. A. Eaton, *J. Mol. Bio.* **183**(4), 611-631 (1985)
[21] J. Hofrichter, *J. Mol. Bio.* **189**(3), 553-571 (1986)
[22] A. Szabo, J. Mol. Bio. **199**(3), 539-542 (1988)
[23] M. R. D'Orsogna, G. Lakatos and T. Chou, *J. Chem. Phys.* **136**, 084110 (2012)
[24] Note that both the deterministic models to which we refer in this paper, and our stochastic model, assume that the system is "well-mixed", i.e. spatially homogeneous.
[25] To derive the coarse-grained model from the full one including fragmentation we have to ignore the fact that any fibril created by fragmentation that is smaller than n_c is considered to be unstable and thus dissolves, adding n_c free monomers to the solution.
[26] C. F. Lee, *Phys. Rev. E* **80**, 031134 (2009)
[27] J. Paturej, A. Milchev, V. G. Rostiashvili and T. A. Vilgis, *J. Chem. Phys.* **134**, 224901 (2011)
[28] J. S. Schreck and J.-M. Yuan, *J. Phys. Chem. B* **117**(21),6574-6583 (2013)
[29] N. G. van Kampen, *Stochastic Processes in Physics and Chemistry* (Elsevier, Amsterdam, 2007)
[30] C. Gardiner, *Stochastic Methods*, (Springer-Verlag, Berlin, 2009)
[31] The variable $r(t)$ has the properties that $r(0) = -\infty$ and $r(T) = 0$; also, $r(\infty)$ is finite and can be calculated by noting that for large times $\psi(t) \approx A\exp(\sqrt{\mu\lambda}t)$ and $\langle x_2^2(t)\rangle \approx C\exp(2\sqrt{\mu\lambda}t)$ yielding $r(\infty) = A/\sqrt{\epsilon C}$.
[32] In Ref. [18], k_+ and k_f were calculated from the speed and width of the aggregation front in the droplets; we also assumed, as in previous work that $n_c = 2$ and $\phi(0) = \psi(0) = 0$ [7, 17].
[33] W.-F. Xue, S. W. Homans and S. E. Radford, *Proc. Natl Acad. Sci. USA* **105**(26), 8926-31 (2008)

Supplemental Material to: Inherent variability in the kinetics of autocatalytic protein self-assembly

EXPERIMENTAL SETUP

To obtain the experimental data shown in Fig. 1(a), bovine insulin was obtained from Sigma-Aldrich (I55004, lot number 0001434060). The zinc content was approximately 0.5% (w/w). The samples in this study were dissolved in 25 mM HCl (pH 1.6) immediately prior to the experiment. All solvents and solutions were filtered through a 0.22 μm filter (Millipore). Concentrations were checked via UV-Vis absorption spectroscopy. ThT was added to each solution to a final concentration of 20 μM. Experiments were conducted using Corning NBS 96-well plates (Corning 3641). These plates are coated with a proprietary PEO-like hydrophilic coating which minimizes the interaction of protein with the plates. It was found that using these plates significantly minimized the variability in the kinetics compared to standard polystyrene microwell plates. Each well of the plate was filled with 100 μL of solution. Experiments were replicated across 2-3 whole plates for each protein concentration. The plates were sealed with a plastic adhesive and then incubated at 60° C. The kinetics of aggregation was followed via the binding of the fluorescent dye Thioflavin T (ThT), which binds preferentially to the fibrillar form of the protein. Fluorescence readings were taken from the bottom optic. The final number of individual experiments for a given protein concentration ranged from $\sim$ 140-200.

In total, 68 replicate kinetic curves at protein concentration of 0.75 mg/mL, at pH 1.6 and 60° C were used to obtain the average growth curve in Fig. 1(a) (solid black line), which was then fitted to the theoretical prediction from [7] (dashed red line)

$$\frac{M(t)}{c_{tot}} = 1 - \exp\left\{-\frac{\alpha}{c_{tot}}\left[\cosh(\sqrt{2k_+c_{tot}k_f}) - 1\right]\right\}, \tag{S1}$$

to obtain the kinetic parameters $n_c = 2$, $\alpha = 5.8 \cdot 10^{-16}$ mol/(l s), $k_+ = 5 \cdot 10^4$ l/(mol s) and $k_f = 3 \cdot 10^{-8}$ s^{-1}. These parameters were used in the simulations of Fig. 1(b).

FULL STOCHASTIC MODEL INVOLVING NUCLEATION, ELONGATION AND FRAGMENTATION

The full stochastic model [17] tracks the number of fibrils n_i for each fibril length $i \geq n_c$, where n_c is the size of the smallest stable fibril. The state of the system is then fully described by the collection of integers $\{n_{n_c}, n_{n_c+1} \ldots, \}$.

The master equation that governs the time evolution for the probability $P(\{n_i\}, t)$ to find the system in a state $\{n_i\}$ is then given by

$$\begin{aligned}\frac{d}{dt}P(\{n_i\}) = &\frac{\alpha(c(t)+n_c\epsilon)}{\epsilon}\theta(n_{n_c}-1)P(\{n_{n_c}-1,\ldots\}) - \frac{\alpha(c(t))}{\epsilon}P(\{n_i\}) \\ &+ 2k_+(c(t)+\epsilon)\sum_{i\geq n_c}(n_i+1)P(\ldots,n_i+1,n_{i+1}-1,\ldots)\theta(n_i+1)\theta(n_{i+1}-1) \\ &- 2k_+c(t)\sum_{i\geq n_c} n_iP(\{n_i\}) + \text{fragmentation terms}\end{aligned} \tag{S2}$$

Here, $c(t)$ is the molar concentration of free monomers, $c(t) = c_{tot} - \sum_{i\geq n_c} in_i\epsilon$, where c_{tot} is the initial monomer concentration, $\epsilon = 1/(VN_A)$, V is the volume and N_A is Avogadro's constant; to account for the allowed transitions between the states, we used the Heaviside step function $\theta(n)$ which equals 0 for $n < 0$ and 1 for $n \geq 0$. The first two terms in Eq. (S2) describe nucleation, the next two elongation and the rest of terms, which we will write below, describe fragmentation.

Now, let us define the total number of fibrils n and the number of monomers in aggregates m, respectively,

$$n = \sum_{i\geq n_c} n_i, \quad m = \sum_{i\geq n_c} in_i.$$

The probability $P(n, m, t)$ to find the system with a particular n and m at time t can be obtained by summing $P(\{n_i\})$ over all states $\{n_i\}$ having $\sum_{i\geq n_c} = n$ and $\sum_{i\geq n_c} in_i = m$, i.e.

$$P(n,m,t) = \sum_{\{n_i\}} P(\{n_i\})\delta(n - \sum_{i\geq n_c} n_i)\delta(m - \sum_{i\geq n_c} in_i), \tag{S3}$$

where $\delta(i,j)$ denotes the Kronecker delta function.

In Eq. (S2), the nucleation and elongation terms both contain the number of free monomers $c(t)$, which is state-dependent. As we are interested in early times only, we can ignore monomer depletion and approximate $c(t)$ with c_{tot}. From there it is straightforward to obtain the master equation for $P(n,m,t)$, which reads

$$\begin{aligned}\frac{d}{dt}P(n,m,t) = (\alpha/\epsilon)P(n-1,m-n_c,t) - (\alpha/\epsilon)P(n,m,t) + 2k_+c_{tot}nP(n,m-1)\\ - 2k_+c_{tot}nP(n,m) + \text{fragmentation terms},\end{aligned} \tag{S4}$$

where we have used the notation $\alpha \equiv \alpha(c_{tot})$.

To write the fragmentation terms, we have to distinguish between fibrils of length $n_c \le i \le 2n_c - 1$ and $i \ge 2n_c$. These two cases differ in the possible ways a fibril can be broken, taking into account the fact that the smallest stable fibril unit has length n_c. If a fibril of length $n_c \le i < 2n_c$ breaks into two fibrils, then at least one of them must be *unstable*, and therefore will dissolve. On the other hand, if a fibril of length $i \ge 2n_c$ breaks into two fibrils, at least one of them must be *stable*. That said, we can write the fragmentation terms on the r.h.s. of the master equation (S2) as

$$\begin{aligned}\text{fragmentation terms} = &\sum_{i=n_c}^{2n_c-1}\sum_{k=1}^{i-n_c} k_f(n_i+1)P(\dots,n_{i-k}-1,\dots,n_i+1,\dots)\theta(n_{i-k}-1)\\
&+\sum_{i=n_c}^{2n_c-1}\sum_{k=n_c}^{i-1} k_f(n_i+1)P(\dots,n_k-1,\dots,n_i+1,\dots)\theta(n_k-1)\\
&+\sum_{i\ge 2n_c}\sum_{k=1}^{n_c-1} k_f(n_i+1)P(\dots,n_{i-k}+1,\dots,n_i+1,\dots)\theta(n_{i-k}-1)\\
&+\sum_{i\ge 2n_c}\sum_{k=i-n_c+1}^{i-1} k_f(n_i+1)P(\dots,n_{i-k}+1,\dots,n_i+1,\dots)\theta(n_k-1)\\
&+\sum_{i=n_c}^{2n_c-2}\sum_{k=i-n_c+1}^{n_c-1} k_f(n_i+1)P(\dots,n_i+1,\dots)\\
&+\sum_{i\ge 2n_c}\sum_{k=n_c}^{i-n_c} k_f(n_i+1)P(\dots,n_k-1,\dots,n_{i-k}-1,\dots,n_i+1,\dots)\theta(n_k-1)\theta(n_{i-k}-1)\\
&-\sum_{i\ge n_c}\sum_{k=1}^{i} k_f n_i P(\{n_i\})\theta(n_i-1)\end{aligned} \tag{S5}$$

The first four terms above describe fragmentation events which produce exactly one unstable fibril; the fifth and the sixth term describe events that produce two unstable and two stable fibrils, respectively. Equation (S2) with the fragmentation terms given in (S5) is the basis of our full stochastic model, which is then compared to the analytical predictions of the simpler, coarse-grained model (in Fig. 2 of the main text).

COARSE-GRAINING THE FULL STOCHASTIC MODEL

To obtain our coarse-grained model, we ignore the occurrences of unstable fibrils. This yields the following master equation for $P_{n,m}(t)$ after summing (S2) and (S5) over all states $\{n_i\}$ with given n and m,

$$\begin{aligned}\frac{d}{dt}P(n,m,t) = (\alpha/\epsilon)P(n-1,m-n_c,t) - (\alpha/\epsilon)P(n,m,t) + 2k_+m_{tot}nP(n,m-1)\\ - 2k_+c_{tot}nP(n,m) + k_f[m-(2n_c-1)(n-1)]P(n-1,m) - k_f[m-(2n_c-1)n]P(n,m,t).\end{aligned} \tag{S6}$$

Except for very early times, m is expected to be much larger than n, and so $m-(2n_c-1)n$ can be approximated by m. This leads to the following master equation,

$$\begin{aligned}\frac{d}{dt}P(n,m,t) = (\alpha/\epsilon)P(n-1,m-n_c,t) - (\alpha/\epsilon)P(n,m,t) + 2k_+c_{tot}nP(n,m-1)\\ - 2k_+c_{tot}nP(n,m) + k_fmP(n-1,m) - k_fmP(n,m,t),\end{aligned} \tag{S7}$$

which is the subject of our theoretical analysis.

FULL STOCHASTIC MODEL RESPECTING DETAILED BALANCE

The coarse-grained model discussed in the text main text takes account of the following three chemical reactions:

$$n_c m \xrightarrow{k_n} F_{n_c}, \tag{S8}$$

$$m + F_i \xrightarrow{k_+} F_{i+1}, \quad i \geq n_c, \tag{S9}$$

$$F_{i+j} \xrightarrow{k_f} F_i + F_j, \quad i,j \geq n_c, \tag{S10}$$

where m denotes a monomer and F_i a fibril of length i. This reaction scheme does not obey detailed balance. To extend our scheme so that it does obey detailed balance, we add the following 'backward' processes

$$F_{n_c} \xrightarrow{k_d} n_c m, \tag{S11}$$

$$F_{i+1} \xrightarrow{k_-} m + F_i, \quad i \geq n_c, \tag{S12}$$

$$F_i + F_j \xrightarrow{k_c} F_{i+j}, \quad i,j \geq n_c, \tag{S13}$$

which represent disintegration, depolymerization and fibril coalescence (end-joining), respectively. Here we assume length-independent kernels for the fragmentation and coalescence processes, which is true for rate-limited reactions. However, reactions (S10) and (S12) together can be understood as an example of inhomogeneous fragmentation in which a fibril is more likely to break at its ends ($k_- > k_f$). In particular, we set $k_- = \kappa k_f$, where $\kappa \approx 1.1$ is chosen in accordance with a recent theoretical study on rupture probabilities along a single polymer chain [27].

The rate equations for the processes (S8)-(S13) read

$$\frac{d}{dt}\rho_1 = (n_c k_d \rho_{n_c} - n_c k_n \rho_1^{n_c}) + \sum_{j=n_c}^{\infty} \left(2k_-\rho_{j+1} - 2k_+\rho_1\rho_j\right), \tag{S14}$$

$$\begin{aligned}\frac{d}{dt}\rho_{n_c} &= (k_n\rho_1^{n_c} - k_d\rho_{n_c}) + (2k_-\rho_{n_c+1} - 2k_+\rho_1\rho_{n_c}) \\ &\quad + \sum_{j=n_c}^{\infty} \left(2k_f\rho_{n_c+j} - 2k_c\rho_{n_c}\rho_j\right),\end{aligned} \tag{S15}$$

$$\begin{aligned}\frac{d}{dt}\rho_i &= (2k_+\rho_1\rho_{i-1} - 2k_-\rho_i) + (2k_-\rho_{i+1} - 2k_+\rho_1\rho_i) \\ &\quad + \sum_{j=n_c}^{\infty} \left(2k_f\rho_{i+j} - 2k_c\rho_i\rho_j\right) + \sum_{j=n_c}^{i-n_c} \left(k_c\rho_i\rho_{i-j} - k_f\rho_i\right), \quad i \geq n_c + 1\end{aligned} \tag{S16}$$

where ρ_1 denotes the monomer concentration and ρ_i denotes the concentration of fibrils of length i (all in units of molar).

Detailed balance can then be implemented by demanding that each of the terms in parentheses vanishes for the equilibrium concentrations ρ_1^{eq} and ρ_i^{eq} for $i \geq n_c$:

$$k_d\rho_{n_c}^{\mathrm{eq}} = k_n(\rho_1^{\mathrm{eq}})^{n_c} \tag{S17}$$

$$k_-\rho_{i+1}^{\mathrm{eq}} = k_+\rho_1^{\mathrm{eq}}\rho_i^{\mathrm{eq}}, \quad i \geq n_c \tag{S18}$$

$$k_f\rho_{i+j}^{\mathrm{eq}} = k_c\rho_i^{\mathrm{eq}}\rho_j^{\mathrm{eq}}, \quad i,j,\geq n_c. \tag{S19}$$

These equations have the following steady-state solution for $i \geq n_c$

$$\rho_i^{\mathrm{eq}} = \frac{k_n(\rho_1^{\mathrm{eq}})^{n_c}}{k_d}\left(\frac{k_+\rho_1^{\mathrm{eq}}}{k_-}\right)^{i-n_c}, \quad i \geq n_c \tag{S20}$$

provided that

$$k_c = k_f\frac{k_d}{k_n}\left(\frac{k_+}{k_-}\right)^{n_c}. \tag{S21}$$

From conservation of mass, $\rho_1^{\rm eq} + \sum_{i=n_c}^{\infty} i\rho_i^{\rm eq} = c_{tot}$, we also have that

$$\left[\frac{k_n(\rho_1^{\rm eq})^{n_c}}{k_d}\right]\left[\frac{n_c}{1-k_+\rho_1^{\rm eq}/k_-} + \frac{k_+\rho_1^{\rm eq}/k_-}{(1-k_+\rho_1^{\rm eq}/k_-)^2}\right] = c_{tot} - \rho_1, \tag{S22}$$

which can be used to determine k_d, yielding

$$k_d = \left[\frac{k_n(\rho_1^{\rm eq})^{n_c}}{c_{tot}-\rho_1}\right]\left[\frac{n_c}{1-k_+\rho_1^{\rm eq}/k_-} + \frac{k_+\rho_1^{\rm eq}/k_-}{(1-k_+\rho_1^{\rm eq}/k_-)^2}\right]. \tag{S23}$$

The only remaining unknown parameter is $\rho_1^{\rm eq}$, which can be related to $\bar{l}$, the mean fibril length in equilibrium, by

$$\bar{l} = \frac{\sum_{i=n_c}^{\infty} i\rho_i^{\rm eq}}{\sum_{i=n_c}^{\infty} \rho_i^{\rm eq}} = n_c + \frac{k_+\rho_1^{\rm eq}/k_-}{1-k_+\rho_1^{\rm eq}/k_-}, \tag{S24}$$

yielding

$$\rho_1^{\rm eq} = \frac{k_-}{k_+}\frac{\bar{l}-n_c}{\bar{l}-n_c+1}. \tag{S25}$$

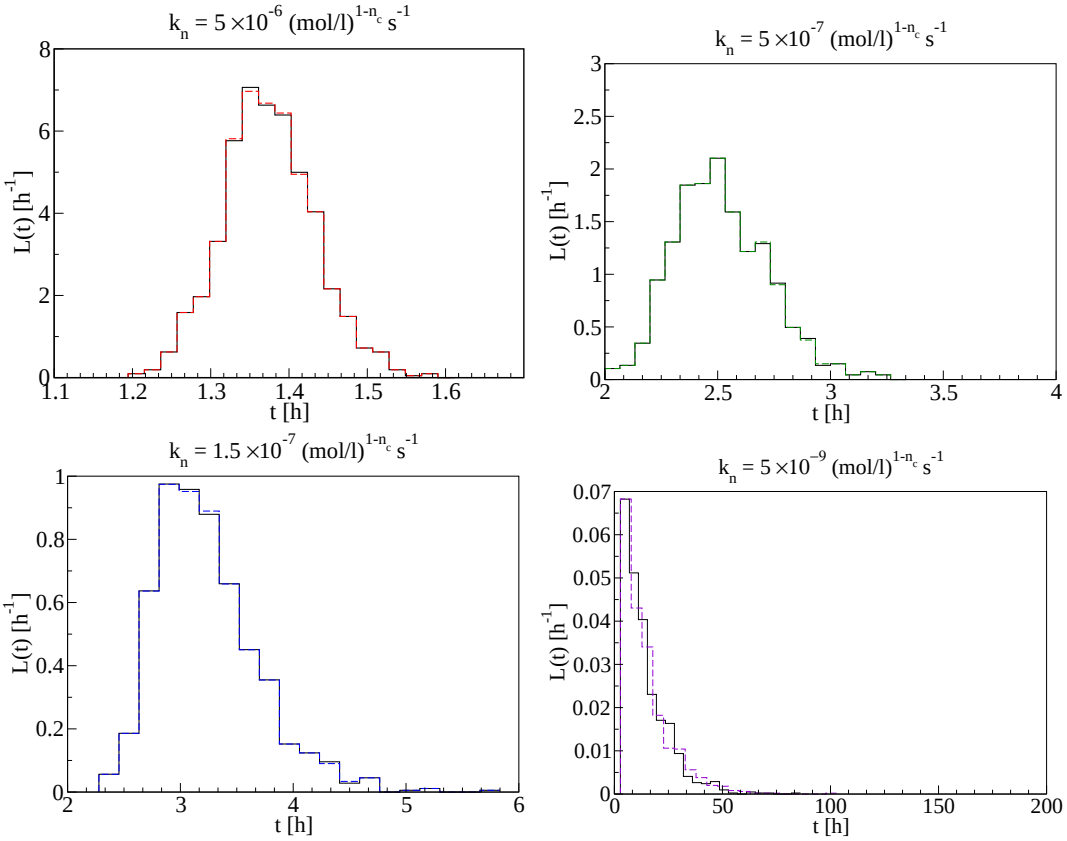

FIG. S1: The lag time distribution for several values of k_n for the model including inhomogeneous fragmentation and respecting detailed balance, compared to the original model including nucleation, elongation and (homogeneous) fragmentation only; all the results were obtained by running 1000 independent kinetic Monte Carlo simulations (using the same random number generator's seeds for both models); see the text below for the values of the other parameters.

Numerical simulations for the stochastic model given by reactions (S8)-(S13) were performed using the Gillespie algorithm for several nucleation rate constants k_n that yield the same values of α as in Fig. 2 in the main text, using the relationship $\alpha = k_n c_{tot}^{n_c}$; the parameters $V = 830$ fl, $M_T = 10\%$ of c_{tot}, $c_{tot} = 100$ μmol/l, $n_c = 2$, $k_+ = 5 \cdot 10^4$ l/(mol s) and $k_f = 3 \cdot 10^{-8}$ s^{-1} were also taken from Fig. 2 in the main text; in addition, the depolymerization rate

was set to $k_- = 1.1k_f = 3.3 \cdot 10^{-8}$ s^{-1}; the value for $\rho_1 = 6.6 \cdot 10^{-13}$ mol/l was obtained using (S25) and setting $\bar{l}$ to 1000; finally, the coalescence and disintegration rates were calculated using (S21) and (S23) respectively for each of the nucleation rate constants.

Results for the lag time distribution are presented in Fig. S1 for the model which includes inhomogeneous fragmentation and respects detailed balance (dashed lines), compared to those for the model analysed in the main text, which assumes homogeneous fragmentation and lacks detailed balance (solid lines). In all four cases the difference between the results of the two models is very small, showing that the effect of inhomogeneous fragmentation and backward processes on the early-time aggregation is negligible. Therefore, the model studied in the main text (Eq. (1)) can safely be used even though it assumes homogeneous fragmentation and neglects detailed balance.

COVARIANCE MATRIX $\Sigma(t)$

For completeness, we list here the other matrix elements of $\Sigma(t)$, $\langle x_1(t)^2\rangle$ and $\langle x_1(t)x_2(v)\rangle$, respectively,

$$\begin{aligned}\langle x_1(t)^2\rangle &= \cosh(2\tau)\left[\frac{1}{6}\left(\Phi_0+\Psi_0\frac{\lambda}{\mu}\right)+\frac{\alpha n_c}{2\mu}\right]+\sinh(2\tau)\sqrt{\frac{\lambda}{\mu}}\left[\frac{\Phi_0+\Psi_0}{3}+\frac{\alpha n_c(n_c-1)}{4\mu}\right]\\ &+\frac{\cosh\tau}{3\mu}\left(\mu\Phi_0-2\lambda\Psi_0\right)+\frac{\sinh\tau}{3}\sqrt{\frac{\lambda}{\mu}}\left(\Psi_0-2\Phi_0\right)-\frac{\lambda}{\mu}\frac{\alpha n_c(n_c-1)t}{2}+\frac{1}{2}\left(\Psi_0\frac{\lambda}{\mu}-\Phi_0-\frac{\alpha n_c}{\mu}\right), \qquad \text{(S26)}\\ \langle x_1(t)x_2(t)\rangle &= \sqrt{\frac{\lambda}{\mu}}\left\{\cosh(2\tau)\sqrt{\frac{\lambda}{\mu}}\frac{\Phi_0+\Psi_0}{3}+\sinh(2\tau)\left[\frac{1}{6}\left(\Phi_0+\Psi_0\frac{\lambda}{\mu}\right)+\frac{\alpha n_c}{2\mu}\right]\right.\\ &\left.-\frac{\cosh\tau}{3}\sqrt{\frac{\lambda}{\mu}}(\Phi_0+\Psi_0)-\frac{\sinh\tau}{3\mu}(\mu\Phi_0+\lambda\Psi_0)\right\}. \qquad \text{(S27)}\end{aligned}$$

CALCULATION OF THE LAG-TIME DISTRIBUTION $L(t)$

to calculate $L(t)$, we first need to find the probability that $m > m_T$ at time t, which is given by

$$\text{Prob}[m > m_T, t] = \int_{-\infty}^{\infty} dx_1 \int_{\frac{m_T\epsilon-\psi(t)}{\sqrt{\epsilon}}}^{\infty} dx_2 P(\vec{x},t). \qquad \text{(S28)}$$

Here $P(\vec{x},t)$ is a bivariate Gaussian distribution with zero mean and covariance matrix Σ,

$$P(\vec{x},t) = \frac{1}{2\pi\sqrt{\det\Sigma}}e^{-\frac{1}{2}\vec{x}^T\Sigma^{-1}\vec{x}}, \quad \Sigma = \begin{pmatrix}\langle x_1(t)^2\rangle & \langle x_1(t)x_2(t)\rangle\\ \langle x_1(t)x_2(t)\rangle & \langle x_2(t)^2\rangle\end{pmatrix}. \qquad \text{(S29)}$$

The argument of the exponential function in (S29) can be expanded as

$$\begin{aligned}\vec{x}^T\Sigma^{-1}\vec{x} &= \frac{\Sigma_{22}x_1^2-2\Sigma_{12}x_1x_2+\Sigma_{11}x_1^2}{\det\Sigma}\\ &= \frac{\Sigma_{22}\left(x_1-\frac{\Sigma_{11}}{\Sigma_{22}}x_2\right)^2}{\det\Sigma}+\frac{1}{\Sigma_{22}}x_2^2. \qquad \text{(S30)}\end{aligned}$$

The integral over x_1 can be easily performed and gives

$$\int_{-\infty}^{\infty} dx_1 \exp\left[-\frac{\Sigma_{22}}{2\det\Sigma}\left(x_1-\frac{\Sigma_{12}}{\Sigma_{22}}x_2\right)^2\right] = \sqrt{\frac{2\pi\det\Sigma}{\Sigma_{22}}}, \qquad \text{(S31)}$$

while the integral over x_2 can be expressed using the complementary error function

$$\begin{aligned}\text{Prob}[m > m_T, t] &= \frac{1}{2\pi\sqrt{\det\Sigma}}\sqrt{\frac{2\pi\det\Sigma}{\Sigma_{22}}}\int_{\frac{m_T\epsilon-\psi(t)}{\sqrt{\epsilon}}}^{\infty} dx_2 e^{-\frac{1}{2\Sigma_{22}}x_2^2} \\ &= \frac{1}{\sqrt{\pi}}\int_{\frac{m_t\epsilon-\psi(t)}{\sqrt{2\epsilon\Sigma_{22}}}} dy e^{-y^2} \\ &= \frac{1}{2}\text{erfc}\left(\frac{m_t\epsilon-\psi(t)}{\sqrt{2\epsilon\Sigma_{22}}}\right). \end{aligned} \tag{S32}$$

Note that our result for $\text{Prob}[m > m_T, t]$ predicts that in general $\text{Prob}[m > m_T, \infty] \neq 1$, i.e. not all trajectories will reach the threshold m_T. We thus have to count only the trajectories where m will reach m_T *eventually*; this amounts to rescaling $\text{Prob}[m > m_T, t]$ with $\text{Prob}[m > m_T, \infty]$.

To find the lag-time distribution $L(t)$, let us look at the probability that $m > m_T$ at time $t + dt$. To find this probability we have to count all events for which $m > m_T$ at time t, plus all the events where m has reached m_T in the time interval $[t, t + dt]$. We can thus write

$$\frac{\text{Prob}[m > m_T, t + dt]}{\text{Prob}[m > m_T, \infty]} = \frac{\text{Prob}[m > m_T, t]}{\text{Prob}[m > m_T, \infty]} + L(t)dt, \tag{S33}$$

from which it follows that

$$L(t) = \frac{\frac{d}{dt}\text{Prob}[m > m_T, t]}{\text{Prob}[m > m_T, \infty]}. \tag{S34}$$

MOMENTS OF THE LAG-TIME DISTRIBUTION $L(t)$

In the main text we defined a new variable r

$$r = \frac{\psi(t) - m_T\epsilon}{\sqrt{\epsilon\langle x_2(t)^2\rangle}}, \tag{S35}$$

such that the lag time distribution $L(t)$ becomes a Gaussian in r,

$$L(t)dt = \frac{dr/dt}{\sqrt{2\pi}Z}e^{-r(t)^2/2} = \frac{1}{\sqrt{2\pi}Z}e^{-r^2/2}dr. \tag{S36}$$

Here r takes values in the range $\langle -\infty, r(\infty)]$, where $r(\infty)$ is given by

$$r(\infty) = \frac{\Psi_0 + (\mu/\lambda)\Phi_0}{\sqrt{\epsilon\{[\Psi_0 + (\mu/\lambda)\Phi_0]/3 + \alpha n_c/\lambda + \sqrt{\mu/\lambda}[(\Psi_0 + \Phi_0)/3 + \alpha n_c(n_c - 1)/(2\mu)]\}}}. \tag{S37}$$

To calculate an average of some physical quantity $w(t)$, we can make a change of variable from t to r,

$$\langle w(t)\rangle = \int_0^\infty dt w(t)L(t) = \frac{1}{\sqrt{2\pi}Z}\int_{-\infty}^{r(\infty)} dr w(r)e^{-r^2/2}. \tag{S38}$$

To complete the calculation, we have to express t as a function of r so that $w(r) = w(t(r))$. However, the final integral in (S38) is unlikely to be analytically tractable, and thus we take a different approach. Using the fact that $r(t = T) = 0$, we can make a Taylor expansion of $w(t(r))$ around $r = 0$,

$$w(t(r)) = w(r) = \sum_{k=0}^{\infty}\frac{w^{(k)}(r = 0)}{k!}r^k, \tag{S39}$$

where $w^{(k)}$ is the k-th derivative with respect to r. Inserting the Taylor expansion (S39) in (S38) we get a formal expression for $\langle w(t)\rangle$ as

$$\langle w(t)\rangle = \sum_{k=0}^{\infty}\frac{w^{(k)}(r = 0)}{k!}\langle r^k\rangle \tag{S40}$$

where $\langle r^k \rangle$ is given by

$$\langle r^k \rangle = \frac{2^{(k-1)/2}}{\sqrt{2\pi}Z}\left[(-1)^k \Gamma\left(\frac{k+1}{2}\right) + \gamma\left(\frac{k+1}{2}, \frac{r(\infty)^2}{2}\right)\right]. \tag{S41}$$

Here $\Gamma(z)$ and $\gamma(z,x)$ are the gamma and lower incomplete gamma functions, respectively. For example, the first few terms are:

$$\langle r \rangle = -\frac{1}{\sqrt{2\pi}Z} e^{-r(\infty)^2/2}, \quad \langle r^2 \rangle = 1 - \frac{r(\infty)}{\sqrt{2\pi}Z} e^{-r(\infty)^2/2}. \tag{S42}$$

For higher-order terms we can use the following recursion relation:

$$\langle r^k \rangle = \langle r^{k-2} \rangle - \frac{r(\infty)^{k-1}}{\sqrt{2\pi}Z} e^{-r(\infty)^2/2}, \quad k \geq 2, \tag{S43}$$

which can be solved yielding

$$\langle r^{2k} \rangle = 1 + \frac{r(\infty)\langle r \rangle (1 - r(\infty)^{2k})}{1 - r(\infty)^2}, \quad k \geq 0, \tag{S44a}$$

$$\langle r^{2k+1} \rangle = \frac{\langle r \rangle (1 - r(\infty)^{2k+2})}{1 - r(\infty)^2}, \quad k \geq 0. \tag{S44b}$$

To complete the calculation of $\langle w(t) \rangle$, we have to calculate the derivatives in (S39) with respect to r, evaluated at $t = T$. These can be found using Faà di Bruno's formula; for example, the first few terms are given by

$$\begin{aligned}
w^{(1)}(r=0) &= w^{(1)}(t=T)t^{(1)}(r=0) \\
w^{(2)}(r=0) &= w^{(2)}(t=T)[t^{(1)}(r=0)]^2 + w^{(1)}(t=T)t^{(2)}(r=0) \\
w^{(3)}(r=0) &= w^{(3)}(t=T)[t^{(1)}(r=0)]^3 + 3w^{(2)}(t=T)t^{(1)}(r=0)t^{(2)}(r=0) + w^{(1)}(t=T)t^{(3)}(r=0),
\end{aligned}$$

where the unknown derivatives $t^{(k)}(r=0)$ can be calculated by setting $w(t) = t$.

By setting $w(t) = t$ and $w(t) = t^2 - \langle t \rangle^2$ we get the following expressions for the mean and standard deviation, respectively

$$\langle t \rangle = T - \frac{e^{-r(\infty)^2/2}}{\sqrt{2\pi}Z r^{(1)}(T)} + \left(1 - \frac{r(\infty)e^{-r(\infty)^2/2}}{\sqrt{2\pi}Z}\right)\frac{r^{(2)}(T)}{2[r^{(1)}(T)]^3} + \ldots, \tag{S45}$$

$$\sigma^2 = \frac{1}{r^{(1)}(T)}\left(1 - \frac{r(\infty)e^{-r(\infty)^2/2}}{\sqrt{2\pi}Z}\right)\left[1 - \frac{Tr^{(2)}(T)}{r^{(1)}(T)} + \frac{Tr^{(2)}(T)}{[r^{(1)}(T)]^2}\right] + \ldots, \tag{S46}$$

where $r^{(k)}(T) = \phi^{(k)}(T)/\sqrt{\epsilon\langle x_2(T) \rangle}$ for $k \geq 1$.